



OPEN ACCESS

EDITED BY

Amar Prasad Misra,
Visva-Bharati University, India

REVIEWED BY

Gert Brodin,
Umeå University, Sweden
Bengt Eliasson,
University of Strathclyde,
United Kingdom

*CORRESPONDENCE

J.T. Mendonça,
titomend@tecnico.ulisboa.pt
J. Vieira,
jorge.vieira@tecnico.ulisboa.pt
C. Willim,
camilla.willim@tecnico.ulisboa.pt
R. Fedele,
renato.fedele@na.infn.it

SPECIALTY SECTION

This article was submitted to Low-Temperature Plasma Physics, a section of the journal Frontiers in Physics

RECEIVED 15 July 2022

ACCEPTED 01 August 2022

PUBLISHED 07 September 2022

CITATION

Mendonça JT, Vieira J, Willim C and Fedele R (2022), Particle acceleration by twisted laser beams. *Front. Phys.* 10:995379. doi: 10.3389/fphy.2022.995379

COPYRIGHT

© 2022 Mendonça, Vieira, Willim and Fedele. This is an open-access article distributed under the terms of the [Creative Commons Attribution License \(CC BY\)](https://creativecommons.org/licenses/by/4.0/). The use, distribution or reproduction in other forums is permitted, provided the original author(s) and the copyright owner(s) are credited and that the original publication in this journal is cited, in accordance with accepted academic practice. No use, distribution or reproduction is permitted which does not comply with these terms.

Particle acceleration by twisted laser beams

J.T. Mendonça^{1*}, J. Vieira^{1*}, C. Willim^{1*} and R. Fedele^{2*}

¹IPFN, Instituto Superior Técnico, Universidade de Lisboa, Lisboa, Portugal, ²Dipartimento di Fisica, Università di Napoli Federico II and INFN Sezione di Napoli, Naples, Italy

We consider particle acceleration in plasmas, using twisted laser beams, or beams with orbital angular momentum. We discuss different acceleration processes using two LG laser modes, which include donut wakefield, beat-wave and self-torque acceleration, and compare the respective properties. We show that a self-torque configuration is able to produce azimuthal acceleration and can therefore be considered as an alternative method to produce helical electron beams.

KEYWORDS

laser-plasma acceleration, helical beams, twisted laser pulses, self-torque, light spring

1 Introduction

Particle acceleration by laser-plasma interactions is a dominant subject in plasma physics, which attracted the attention of several researchers over the last few decades (see the review papers [1, 2]). In this vast area of research, different acceleration schemes were explored, among them the beat-wave and the wakefield acceleration. Here, these two concepts will be compared using twisted laser pulses as the drivers of the plasma acceleration process. Beat-wave acceleration assumes the use of two long laser beams, with durations much larger than the electron plasma period and a frequency difference equal to the electron plasma frequency [3, 4]. This concept was the first to attract the attention of the experimentalists, and led to the first evidence of plasma acceleration [5]. In contrast, the wakefield concept relies on the use of more intense and shorter laser pulses, with durations smaller than the electron plasma period [6]. This acceleration scheme led to impressive experimental results in the recent years and can be seen as a precursor to future high-energy accelerators [7, 8].

In recent years, a new variant of wakefield acceleration was proposed, making use of twisted laser pulses as drivers of plasma waves carrying a finite amount of orbital angular momentum [12, 13]. These twisted laser pulses can be described by Laguerre-Gauss (LG) modes [10, 11], and are able to excite donut shaped electron plasma wakes [12], in a configuration that seems adequate to accelerate electron beams with a hollow cylindrical profile [13]. Furthermore, efficient acceleration of positrons also seems possible. If, instead of a single mode, two or more LG laser modes are used, it is then possible to excite helical plasma perturbations and to accelerate helical electron beams [14]. This new laser driver is sometimes called a light spring.

Twisted plasma waves were introduced in plasma physics recently [9]. They can be understood as a natural extension of twisted photons, previously considered in optics [10,

11], because plasmons correspond to electrostatic photons, or in other words, to photons in a state of zero spin. In a sense, they generalize the concept of twisted photons to include all the three available spin states ($s = 0, \pm 1$), given that the $s = \pm 1$ spin states correspond to circularly polarized transverse photons, and zero spin state $s = 0$ to plasmons. They can only exist in media with free electron populations, such as plasmas, semiconductors and metals.

Here, we return to the case of wakefields generated by two-mode laser pulses. We show that this simple laser driver can excite at least three types of wakes, which can be called donut wakes, self-torque and light springs. In particular, we show that self-torque wakes can lead to helical acceleration, similar to that observed in light-springs. We also show that, for long pulses, the light-spring case can be seen as a twisted version of the beat-wave acceleration scheme. Therefore, we can observe a transition from the beat-wave to the wakefield acceleration simply by changing the laser pulse duration, or equivalently, by changing the plasma frequency.

2 Basic equations

We start with the electron fluid equations describing the slow plasma response to the laser beams. They determine the electron density n and velocity \mathbf{v} produced by a laser pulse, and can be written in relativistic form as [12].

$$\frac{Dn}{Dt} + cn_0 \nabla \cdot \mathbf{u} \gamma = 0, \tag{1}$$

and

$$\frac{D\mathbf{u}}{Dt} = c \nabla \phi - \frac{c}{2} \left\langle \frac{\nabla a^2}{\gamma} \right\rangle. \tag{2}$$

where we have used the differential operator

$$\frac{D}{Dt} \equiv \frac{\partial}{\partial t} + \frac{c}{\gamma} (\mathbf{u} \cdot \nabla). \tag{3}$$

We also use the covariant electron velocity $\mathbf{u} = \gamma \mathbf{v}/c$ and the relativistic factor $\gamma = \sqrt{1 + u^2}$. The notation $\langle \rangle$ represents an average over a time interval larger than the laser period, and shorter than the electron plasma period. In the momentum Eq. 2 we have neglected the electron pressure term, which is valid for intense pulses, when the electron quiver velocity associated with the laser field is much larger than the electron thermal velocity. The normalized scalar potential, ϕ , describing the slow plasma perturbation, and vector potential \mathbf{a} associated with the laser field, are defined by the expressions

$$\phi = \frac{eV}{mc^2}, \quad \mathbf{a} = \frac{e\mathbf{A}}{mc}, \tag{4}$$

where V and \mathbf{A} are the usual potentials, assumed in the Coulomb gauge. The corresponding electric and magnetic fields are determined by

$$\mathbf{E} = -\frac{mc}{e} \left(\frac{\partial \mathbf{a}}{\partial t} + c \nabla \phi \right), \quad \mathbf{B} = \frac{mc}{e} (\nabla \times \mathbf{a}). \tag{5}$$

From the fluid Equations 1, 2, we can derive, to the lowest order, an equation for the density perturbations $\tilde{n} = n - n_0$ created by the laser pulses, as

$$\left(\frac{\partial^2}{\partial t^2} + \omega_p^2 \right) \tilde{n} = \frac{c^2}{2} n_0 \nabla \cdot \left\langle \frac{\nabla a^2}{\gamma_a} \right\rangle. \tag{6}$$

where the relativistic factor $\gamma \approx \gamma_a = \sqrt{1 + a^2}$, valid in the laser pulse region [12], was used in the driving term. Notice that a similar relativistic factor should appear in the term containing the electron plasma frequency $\omega_p = (e^2 n_0 / \epsilon_0 m)^{1/2}$, due to the increase of the effective electron mass. This is ignored here by assuming that the density perturbation associated with the laser pulse mainly occurs in the region behind the pulse, where $a^2 \sim 0$. For this reason, the relativistic mass corrections are only significant for the driving force term. We now assume that the laser pulse is described by a superposition of different Laguerre-Gauss (LG) field modes, eventually with different frequency components ω_ν . They can be represented as

$$\mathbf{a}(\mathbf{r}, t) = \sum_\nu \mathbf{a}_\nu F_\nu(r, \theta) \exp(i\mathbf{k}_\nu \cdot \mathbf{r} - i\omega_\nu t) + c.c., \tag{7}$$

where $\nu \equiv (p, \ell)$ represent the pairs of integers representing the different LG modes, and the corresponding mode functions describe their transverse structure and are determined by the well known expressions

$$F_\nu(r, \theta) \equiv F_{p\ell} = C_{p\ell} X^{|\ell|/2} L_p^{|\ell|}(X) \exp\left(i\ell\theta - \frac{X}{2}\right), \tag{8}$$

where L_p^ℓ are the associated Laguerre polynomials of argument $X = r^2/w^2$, where $w \equiv w(z)$ is the laser beam waist, which is allowed to evolve slowly along propagation. The normalization constant $C_{p\ell}$ is chosen to allow orthonormality, as defined by the condition

$$\int_0^\infty r dr \int_0^{2\pi} d\theta F_{p\ell} F_{p'\ell'} = \delta_{pp'} \delta_{\ell\ell'}. \tag{9}$$

Occasionally, we will also use the notation $F_\nu(r, \theta) = F_\nu(r) e^{i\ell\theta}$. Let us now use the field Equation 7 to calculate the ponderomotive force appearing in Eq. 6. For that purpose, we focus on the case of two LG modes, $\nu = 1, 2$, which is sufficient to illustrate the main differences between the beat-wave and wakefield acceleration schemes, and to explore different wakefield configurations, such as the donut, self-torque and light-spring configurations. We then have

$$a^2 = \sum_{\nu=1,2} |a_j(\eta_\nu) F_\nu(r)|^2 + 2(\mathbf{a}_1 \cdot \mathbf{a}_2^*) |F_1(r)| |F_2(r)| \cos(\Delta k z + \Delta \ell \theta - \Delta \omega t), \tag{10}$$

with $\Delta k = k_1 - k_2$, $\Delta \ell = \ell - \ell'$ and $\Delta \omega = \omega_1 - \omega_2$. We have also used the space-time variables $\eta_\nu = z - \nu_\nu t$, where ν_ν are the group

velocities of the two LG modes. For very similar mode frequencies, $\omega_1 \sim \omega_2$, we can use a single space-time variable $\eta_1 \sim \eta_2 = \eta$.

3 Twisted wakes

In order to solve Eq. 6, we can use the decomposition of the density perturbations \tilde{n} in LG mode components, as

$$\tilde{n}(\mathbf{r}, t) = \sum_{p'\ell'} N_{p'\ell'}(z, t) F_{p'\ell'}(r, \theta), \tag{11}$$

Replacing this in Eq. 6, we would get an equation for each density mode component, $N_{p\ell}$. This approach was followed in [12]. An alternative approach is to use the decomposition into the principal components, according to

$$\tilde{n}(\mathbf{r}, t) = \sum_{\nu=1,2} N_{\nu}(z, t) |F_{\nu}(r)|^2 + N_3(z, t) F_1(r) F_2(r), \tag{12}$$

In this case, we can derive three independent equations for the N_{ν} and N_3 , associated with the principal components of the wakefield perturbations, as

$$\left(\frac{\partial^2}{\partial t^2} + \omega_p^2\right) N_{\nu} = \frac{c^2}{2} n_0 \frac{\partial}{\partial z} \left(\frac{1}{\gamma_a} \frac{\partial}{\partial z} a_{\nu}^2\right). \tag{13}$$

for $\nu = 1, 2$, and

$$\left(\frac{\partial^2}{\partial t^2} + \omega_p^2\right) N_3 = \frac{c^2}{2} n_0 \frac{\partial}{\partial z} \left[\frac{1}{\gamma_a} \frac{\partial}{\partial z} a_1 a_2^* \cos(\Delta k z + \Delta \ell \theta - \Delta \omega t)\right]. \tag{14}$$

Here, we have assumed that $\nabla^2 \approx \partial^2/\partial z^2$. But the radial corrections associated with ∇_{\perp}^2 would not introduce relevant qualitative changes in the wakefield solutions [12]. We now use these evolution equations to discuss three different wakefield configurations.

3.1 Donut wakes

In this case, we only have a single LG laser mode, $a \equiv a_1$, with $a_2 = 0$. To simplify the discussion we assume the weakly relativistic case, $\gamma_a \sim 1$, and write

$$\left(\frac{\partial^2}{\partial \eta^2} + k_p^2\right) N_{\nu} = \frac{\partial^2}{\partial \eta^2} V_1(\eta). \tag{15}$$

and

$$V_1(\eta) = \frac{n_0}{2} |a_1(\eta)|^2, \tag{16}$$

where $k_p = \omega_p/v_1$, $\eta = z - v_1 t$, and $v_1 = \partial\omega_1/\partial k_1 = c$ is the laser pulse group velocity. This can easily be integrated, leading to

$$N_1(\eta) = \delta N_1(\eta) - \int_{\eta_0}^{\eta} V_1(\eta') \sin[k_p(\eta - \eta')] d\eta', \tag{17}$$

with

$$\delta N_1(\eta) = V_1(\eta) - V_1(\eta_0) \cos(k_p \eta) - \left(\frac{\partial V_1}{\partial \eta}\right)_{\eta_0} \sin(k_p \eta). \tag{18}$$

Notice that, far away from the pulse, we can use the initial conditions $V_1(\eta_0) = 0$ and $(\partial V_1/\partial \eta)_{\eta_0} \approx 0$. This allows us to write the donut wakefield solution in terms of the co-moving variable η as

$$\tilde{n}(r, \eta) = \frac{n_0}{2} \left\{ |a_1(\eta)|^2 - \int_{\eta_0}^{\eta} |a_1(\eta')|^2 \sin[k_p(\eta - \eta')] d\eta' \right\} |F_1(r)|^2, \tag{19}$$

where $F_1(r) \equiv F_{p\ell}(r)$. In this solution, the dependence on the azimuthal variable θ vanishes, as illustrated in Figure 1, where the absolute value of the density perturbations associated with the different wakefield configurations are shown. This was previously studied in [12], but here we obtain an explicit solution, and not just a simulation result.

3.2 Self-torque

We now consider the superposition of two distinct LG laser modes, with different values of ℓ but the same frequency. In this case, we have $\Delta \ell \neq 0$, and $\Delta \omega = \Delta k = 0$. We also assume that the envelopes of the two LG modes are displaced in time. For Gaussian pulse envelopes with the same amplitude, we can use

$$a_{\eta}(\eta) = a_0 \exp\left[-\frac{(\eta - \eta_0)^2}{2\sigma^2}\right], \tag{20}$$

for $\nu = 1, 2$ and where, typically, we have $(\eta_1 - \eta_2) \geq \sigma$. This means that the two modes are able to produce two similar but nearly non-overlapping wakes which only slightly distort the above single mode wakefield. Instead of Eqs. 15, 16, we should now use $\gamma_a \sim 1$, and write

$$\left(\frac{\partial^2}{\partial \eta^2} + k_p^2\right) \tilde{n}(\mathbf{r}_{\perp}, \eta) = \frac{\partial^2}{\partial \eta^2} V(\mathbf{r}_{\perp}, \eta). \tag{21}$$

and

$$V(\mathbf{r}_{\perp}, \eta) = \frac{n_0}{2} |a_1(\eta) F_1(r) + a_2(\eta) F_2(r) e^{i\Delta \ell \theta}|^2, \tag{22}$$

where $\mathbf{r}_{\perp} \equiv (r, \theta)$. It should be noticed that, when the mode overlapping is significant, i.e. $(\eta_1 - \eta_2) < \sigma$, these double donut wakes are replaced by a moon-shaped wake. Here, we should note that the creation of such a moon-shaped wake is only significant for $\Delta \ell \ll \ell_{\nu}$, because the radial size of the pulse depends on the azimuthal number ℓ . This is illustrated in Figure 2, where the cases of $(\ell_1 = 1, \ell_2 = 2)$ are represented. Only the first wake is shown. We need to use $a_1 \gg a_2$ in order to observe a significant superposition of the two modes. For comparison, we can see the case of Figure 1 (b), where large azimuthal numbers are considered, $(\ell_1 =$

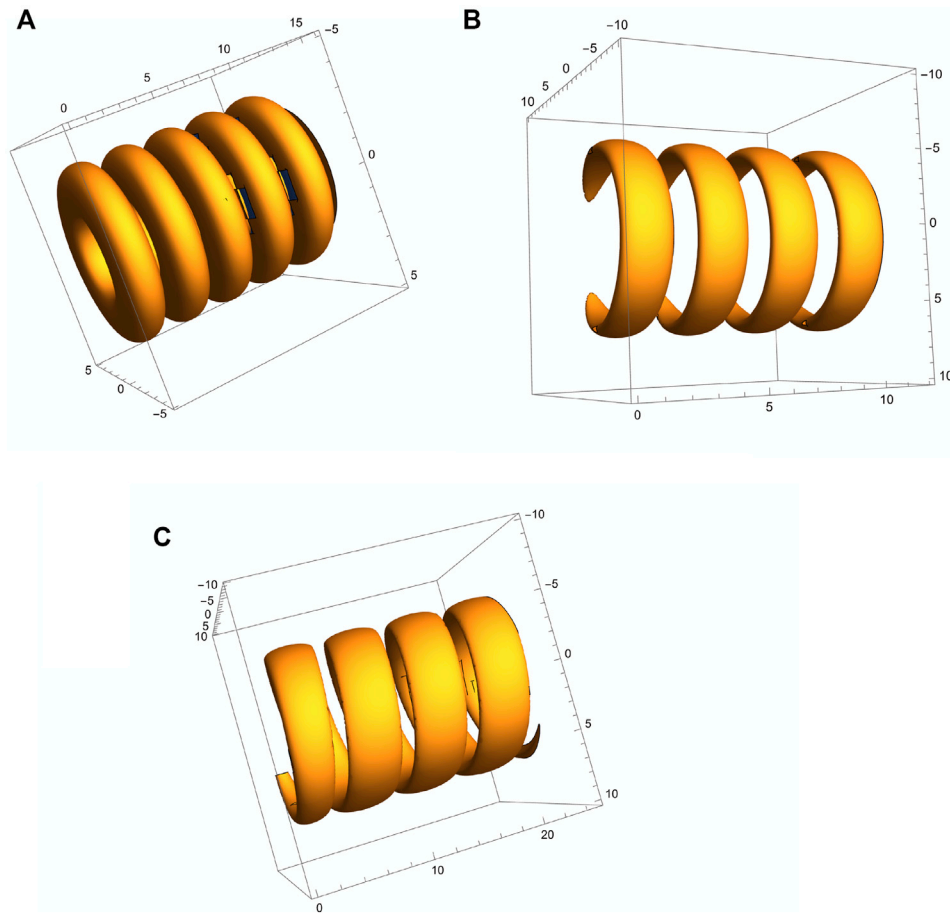


FIGURE 1
 Wakefield configurations: **(A)**–Donut wake, excited by a single LG laser mode with azimuthal index $l = 1$; **(B)**–self-torque wake, produced by a near-superposition of two LG laser modes l_1 and l_2 with the same frequency $\omega_0 \gg \omega_p$ (self-torque configuration); **(C)**–Light-spring, produced by an exact superposition of two LG modes $l_1 = 7$ and $l_2 = 8$, with different frequencies, $\omega_1 \neq \omega_2$. At plasma resonance, $\omega_2 - \omega_1 \approx \omega_p$ this is the generalised beat-wave configuration.

7, $l_2 = 8$) and mode superposition is observed for equal amplitudes $a_1 = a_2$. Transition from a donut shape to a moon-shape configuration is clearly displayed in Figure 2, for different values of $(\eta_1 - \eta_2)$. The consequences of the resulting electron beam structure is considered later.

3.3 Light springs

This new configuration can be achieved with a superposition of two LG laser modes, but now using $\eta_1 = \eta_2$ and $\Delta\omega \approx \omega_p$. Due to this frequency difference, the resulting density perturbations have a helical shape and can be described by Eq. 21, but where Eq. 22 is replaced by a similar, but not identical driving potential

$$V(\mathbf{r}_\perp, \eta) = \frac{n_0}{2} |a(\eta)|^2 |F_1(r) + F_2(r) \exp(i\Delta\ell\theta + i\Delta k\eta)|^2, \quad (23)$$

where $\Delta k \approx k_p$, and $a_1(\eta) = a_2(\eta)$ was assumed. Notice that the density perturbations will mainly be due to the cross-field term, which oscillates at k_p , and as a result, the plasma response will be resonant. The importance of this resonant term will be discussed later in more detail. Notably, we stress the similarity of the light spring configuration with the beat-wave acceleration concept. Therefore, it establishes a bridge between two otherwise distinct acceleration concepts.

4 Acceleration fields

Let us now consider the accelerating electrostatic fields resulting from the above mentioned density perturbations. They are determined by the Poisson’s equation

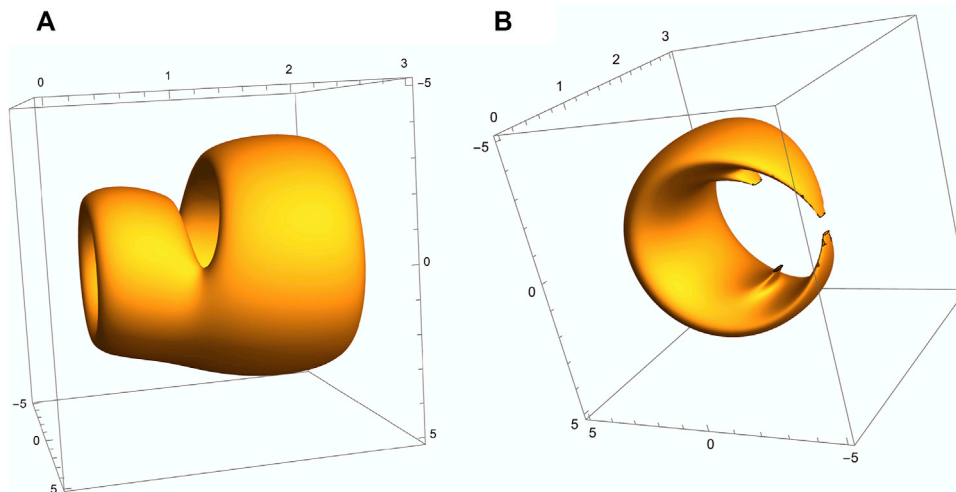


FIGURE 2 Mode superposition for self-torque pulses with large amplitude differences, ($a_1/a_2 = 10$) for small quantum numbers ($\ell_1 = 1, \ell_2 = 2$), for (A) - large time difference ($\eta_1 - \eta_2 = 3$); (B) - for complete superposition ($\eta_1 = \eta_2$).

$$\nabla \cdot \mathbf{E} = -\frac{e}{\epsilon_0} \tilde{n}. \tag{24}$$

The direct influence of the laser field in the acceleration process is ignored, to simplify the discussion. This is strictly valid for short laser driving pulses. Comparing Eq. 24 with Eq. 6, we can easily conclude that

$$\left(\frac{\partial^2}{\partial t^2} + \omega_p^2\right)\mathbf{E} = -\frac{ec^2 n_0}{2\epsilon_0} \left\langle \frac{\nabla a^2}{\gamma_a} \right\rangle. \tag{25}$$

This can be solved using a similar decomposition into the principal field components. It means that, for the axial electric field E_z , we get

$$E_z(\mathbf{r}, t) = \sum_{\nu} E_{z\nu} |F_{\nu}(r)|^2 + E_{z3} |F_1(r)F_2(r)|^2, \tag{26}$$

where the electric field amplitudes are determined by three wakefield equations of the form

$$\left(\frac{\partial^2}{\partial \eta^2} + k_p^2\right)\tilde{E}_{z\nu} = -\frac{\partial}{\partial \eta} \phi_{\nu}(\mathbf{r}_{\perp}, \eta). \tag{27}$$

For the first two components of Eq. 25, where $\nu = 1, 2$, we use the potential functions

$$\phi_{\nu}(\eta) = \frac{en_0}{2\epsilon_0 \gamma_a} a_{\nu}^2, \tag{28}$$

while, for the third one, $\nu = 3$, we have

$$\phi(\eta) = \frac{en_0}{2\epsilon_0 \gamma_a} a_1 a_2^* \cos(\eta + \Delta\ell\theta). \tag{29}$$

Solutions can be derived, as for the density perturbations, and take the form

$$E_{z\nu}(\eta) = \int_{\eta_0}^{\eta} \phi_{\nu}(\eta') \cos(\eta - \eta') d\eta'. \tag{30}$$

The cases $\nu = 1, 2$ take the form of the cylindrical acceleration fields already discussed in [13]. The case $\nu = 3$ is more interesting, and can be written more explicitly as

$$E_{z3}(\eta, \theta) \approx -\frac{en_0}{2\epsilon_0 \gamma_0} (a_1 a_2^*) \int_{\eta_0}^{\eta} \cos(k_p \eta' + \Delta\ell\theta) \cos[k_p(\eta - \eta')] d\eta'. \tag{31}$$

where we have used an averaged value of the relativistic gamma factor inside the pulse, $\gamma_0 \sim \gamma_a$. We can see that, for the case of a self-torque pulse, the resonant part of the potential in η is absent, and we are reduced to

$$E_{z3}(\eta, \theta) \approx -\frac{en_0}{2\epsilon_0 \gamma_0} (a_1 a_2^*) \cos(\Delta\ell\theta) \int_{\eta_0}^{\eta} \cos[k_p(\eta - \eta')] d\eta'. \tag{32}$$

which, apart from the dependence in the azimuthal angle θ , is formally identical to the fields with $\nu = 1, 2$. In Figure 3 we compare the axial electric field component E_{z3} , resulting from short and long laser pulses. We can see that for a short pulse duration, $\Delta t \leq 2\pi/\omega_p$, this accelerating field is similar to that resulting from the usual wakefield acceleration, where the resonant effect associated with the laser mode frequency difference $\Delta\omega \approx \omega_p$ is not relevant. In this case, the light spring configuration studied in [14] is only marginal different than the usual single mode wakefield, apart from the fact that it can produce helical acceleration. But, on the other hand, the self-torque beam, where resonant effects are absent, $\Delta\omega \approx 0$, helical acceleration becomes possible, as shown next.

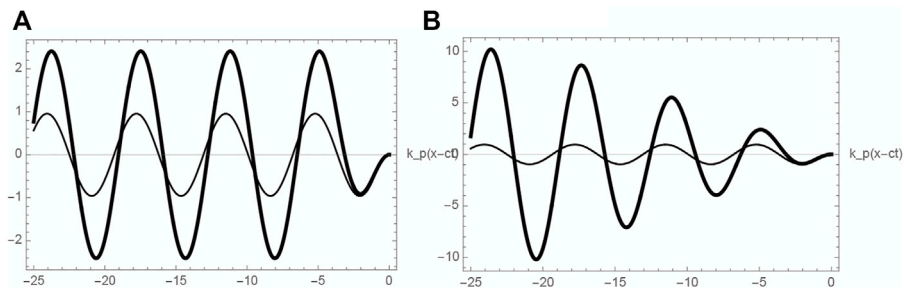


FIGURE 3 Axial wakefield field E_{z3} , for three different values of the laser pulse duration: **(A)** comparison between a short pulse with $\Delta t = 2\pi/\omega_p$, and an intermediate pulse ($\Delta t = 10\pi/\omega_p$, in bold); **(B)** comparison between the short pulse case $\Delta t = 2\pi/\omega_p$ with a very long pulse ($\Delta t = 40\pi/\omega_p$, in bold).

As for the field components in the perpendicular directions, we can use the Panofsky-Wenzel theorem [16], valid for fast charged particle beams. Assuming that an electron beam is formed inside the wake, and that the theorem still applies in these more complex geometries, we can state that

$$\nabla_{\perp} E_z = \frac{\partial}{\partial \eta} W_{\perp}, \quad W_{\perp} = \mathbf{E}_{\perp} + c(\mathbf{e}_z \times \mathbf{B}_{\perp}) \quad (33)$$

where \mathbf{B}_{\perp} is the magnetic field associated with the electron beam. For a dilute beam, it can be neglected. This allows us to calculate an azimuthal field component E_{θ} such that

$$\frac{1}{r} \frac{\partial}{\partial \theta} E_z = \frac{\partial}{\partial \eta} (E_{\theta} + cB_r), \quad (34)$$

which leads to

$$E_{\theta} + cB_r = \frac{\Delta \ell}{r} \int E_z(\eta) d\eta. \quad (35)$$

The existence of an azimuthal field E_{θ} leads to electron acceleration in the transverse direction, and eventually produces helical electron beams. Notice that these helical beams can be produced, not only by light springs as already demonstrated [14], but also by self-torque laser pulses where beat-wave effects are completely absent. This interesting property is one of the main results of the present work.

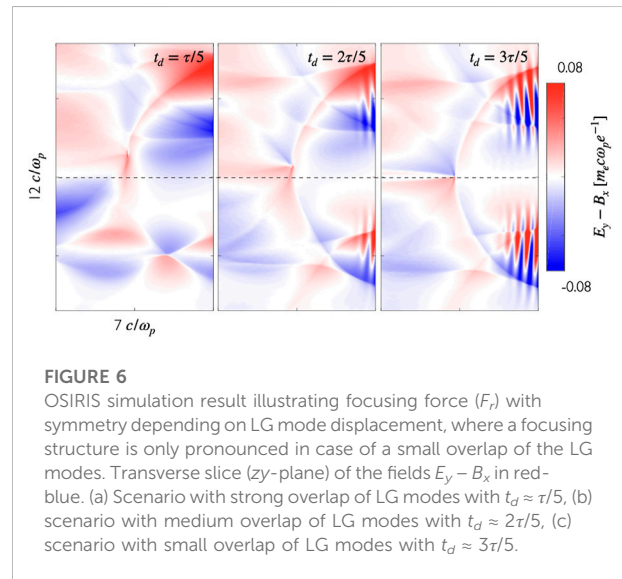
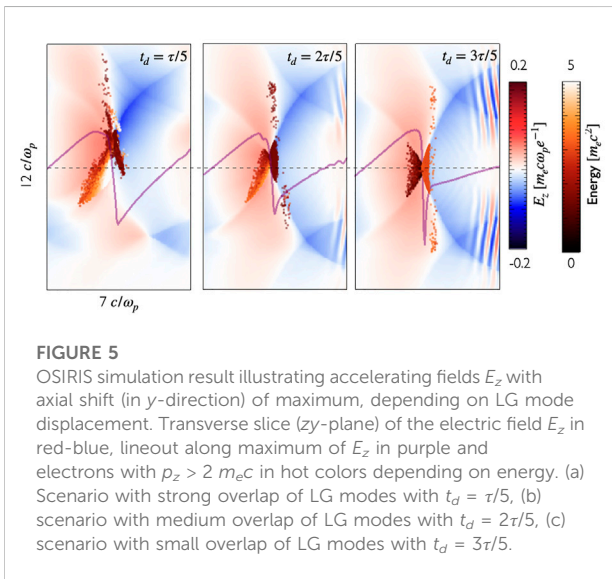
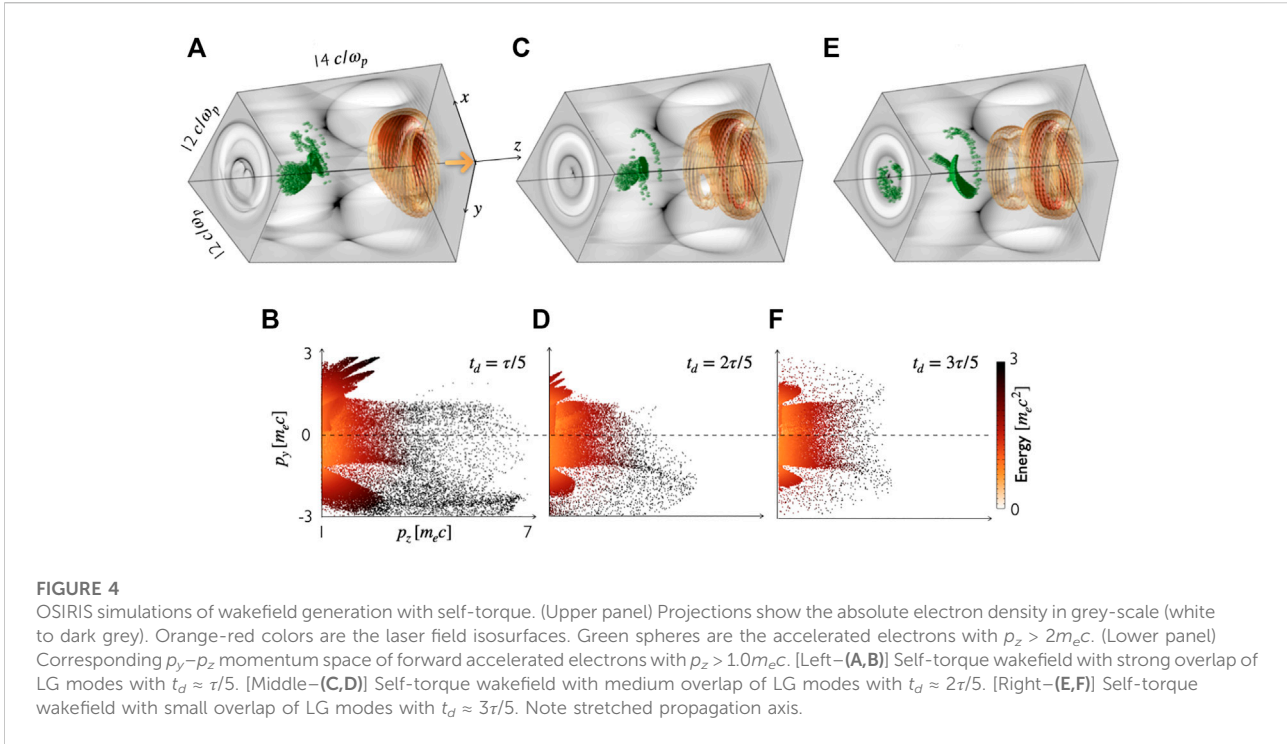
5 Simulation results

Our simulations were mainly focused on the self-torque regime, which was not considered in previous work. We designed a set of three-dimensional simulations, using the particle-in-cell code OSIRIS [15], that support the above predictions for self-torque laser wakefield acceleration and the generation of a quasi-helical electron beam. We tested three scenarios; first, the scenario with a substantial overlap of LG modes that generate a moon-shaped wake, second and third, the

scenarios with less overlap of the LG modes that lead to the formation of a helical electron beam. Figure 4 shows simulation results using a superposition of two linearly polarized (in y -direction) LG modes with $(l_1 = 5, l_2 = 6, p_{1,2} = 0)$, same laser intensity $a_0 = 1.5$ and beam waist $w_0 = 2 c/\omega_p$, pulse duration of $\tau = 5/\omega_p$ with temporal delay between modes of $t_d = 1/\omega_p$ (first simulation with strong overlap), $t_d = 2/\omega_p$ (second simulation with medium overlap), $t_d = 3/\omega_p$ (third simulation with small overlap) and $\omega_0/\omega_p \approx 14$. The simulation uses a moving window propagating at c , with dimensions $14 \times 14 \times 14 c/\omega_p$, divided into $1000 \times 500 \times 500$ cells with $2 \times 1 \times 1$ particles per cell.

Figure 4A shows a self-torque laser consisting of LG modes with strong overlap and corresponding asymmetric moon-shaped wakefield. The bubble is asymmetric with a transversely shifted maximum electron density (dark grey area in projection), where the laser field (orange-red isosurfaces) is maximum. The asymmetry is also found in the electrons with $p_z > 2 m_e c$ (green spheres) along y -direction. In Figure 4B the corresponding momentum space p_y - p_z demonstrates that most electrons accelerate with an asymmetric distribution with respect to p_y , as a result of the asymmetric bubble shape. Interestingly, with less overlap of the LG modes (Figures 4C,E), electron beams with near-helical shape are formed. The corresponding momentum spaces p_y - p_z (Figures 4D,F) demonstrate growing axial symmetry for increased displacement of the LG modes $t_d = 2\pi/5$ to $t_d = 3\pi/5$, but less momentum gain in laser propagation direction p_z .

The accelerating fields E_z of the three scenarios for self-torque wakefield acceleration illustrate electrons where the accelerating field is maximum. The maximum is shifted along y -direction depending on the displacement of the LG-modes. Figure 5 (a) shows a transversely shifted maximum of E_z for $t_d = \pi/5$ and electron acceleration (green dots) in negative y -direction. The more the LG modes are displaced [Figure 5 (b) and (c)], the closer the maximum of E_z moves inwards to the laser propagation axis. The electron distribution is increasingly symmetric and the lineout of E_z shows an increasingly

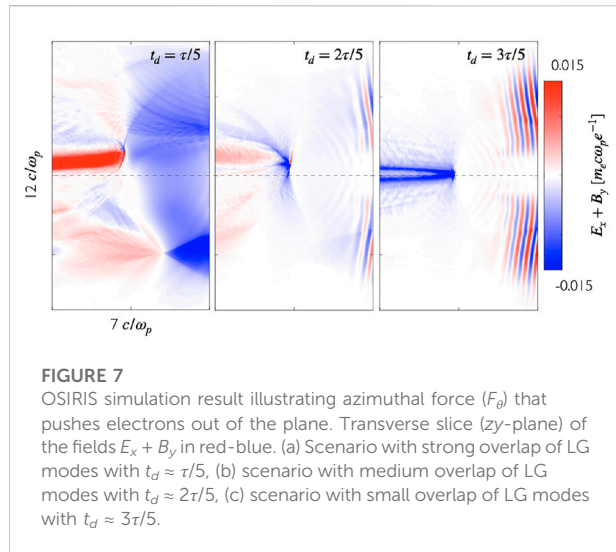


pronounced spike at the bubble back, as expected for a cylindrical symmetric plasma wake.

The corresponding focusing fields $E_y - B_x$ in Figure 6 demonstrate a symmetry dependence on the displacement of the LG modes. Only for the scenario of increased displacement of the LG modes with $t_d = 3\tau/5$ (Figure 6 (c)) we find clear electron focusing fields for the accelerated particles. For stronger overlap,

the asymmetries lead to a less well defined structure that will likely increase beam divergence during acceleration. Figure 7 illustrates the azimuthal fields $E_\theta - B_r$ that push the electrons out of the plane, and confirms the existence of an azimuthal field E_θ (E_x in z, y -plane) as predicted (see Eq. 35).

The combined longitudinal and transverse wakefield structure has a strong influence on the early acceleration stages. This way,



simulations have shown stronger electron acceleration in laser propagation direction (z) in case of a strong overlap of LG modes with $t_d = \pi/5$. However, due to the asymmetry of the moon-shaped wake, electrons also accelerate transversely (in y -direction/laser polarization direction) and because their longitudinal momentum is still below the laser group velocity ($v_g/c \approx 1 - \omega_p^2/2\omega_0^2$) exit the bubble where the accelerating field is the smallest. With increasing displacement of the LG modes, from $t_d = 2\pi/5$ to $t_d = 3\pi/5$, the accelerating fields, focusing fields and azimuthal fields become more symmetric. This leads to electron acceleration close to the propagation axis and the formation of helical electron beams.

6 Conclusion

In this paper, we have studied the three different wakefield configurations that can be obtained with a superposition of two LG laser modes. They correspond to the cases of donut wakes and helical wakes, already considered in the literature and a new configuration called self-torque. The helical wakes are associated with the so-called light-spring laser beams.

We have compared the properties of these three configurations and have shown that they are described by similar expressions for the density perturbations and for the resulting electrostatic field. We have shown that the use of twisted laser beams, described by these LG modes, allows us to establish the bridge between the beat-wave and the wakefield acceleration schemes. The light spring configuration can be seen as beat-wave when twisted laser beams are used. The resonant driving term,

oscillating at the plasma frequency is only relevant for pulses with a duration larger than the electron plasma period, otherwise its resonant character becomes ineffective, as shown here. Furthermore, we were able to show that helical electron beams can also be accelerated by self-torque wakes, where this resonant effect is absent. On the other hand, the temporal difference between the two LG modes with a self-torque can be considered as an additional free parameter which can be used to tune the shape of the helical acceleration.

We hope that this work will contribute to the physical understanding of twisted waves in plasmas, and in particular of the corresponding acceleration processes.

Data availability statement

The original contributions presented in the study are included in the article/Supplementary Material, further inquiries can be directed to the corresponding authors.

Author contributions

All authors listed have made a substantial, direct, and intellectual contribution to the work and approved it for publication.

Funding

This research was partly funded by Fundação para a Ciência e Tecnologia (Portugal), grant number SFRH/IF/01635/2015.

Conflict of interest

The authors declare that the research was conducted in the absence of any commercial or financial relationships that could be construed as a potential conflict of interest.

Publisher's note

All claims expressed in this article are solely those of the authors and do not necessarily represent those of their affiliated organizations, or those of the publisher, the editors and the reviewers. Any product that may be evaluated in this article, or claim that may be made by its manufacturer, is not guaranteed or endorsed by the publisher.

References

1. Bingham R, Mendonça JT, Shukla PK. Plasma based charged-particle accelerators. *Plasma Phys Control Fusion* (2004) 46:R1–R23. doi:10.1088/0741-3335/46/1/r01
2. Esarey E, Schroeder CB, Leemans WP. Physics of laser-driven plasma-based electron accelerators. *Rev Mod Phys* (2009) 81:1229–85. doi:10.1103/revmodphys.81.1229
3. Rosenbluth MN, Liu CS. Excitation of plasma waves by two laser beams. *Phys Rev Lett* (1972) 29:701. doi:10.1103/PhysRevLett.29.701
4. Fedele R, de Angelis U, Katsouleas T. Generation of radial fields in the beat-wave accelerator for Gaussian pump profiles. *Phys Rev A (Coll Park)* (1986) 33:4412–4. doi:10.1103/physreva.33.4412
5. Amiranoff F, Bernard D, Cros B, Jacquet F, Matthieussent G, Mine P, et al. Electron acceleration in Nd-laser plasma beat-wave experiments. *Phys Rev Lett* (1995) 74:5220–3. doi:10.1103/physrevlett.74.5220
6. Tajima T, Dawson JM. Laser electron accelerator. *Phys Rev Lett* (1979) 43:267–70. doi:10.1103/physrevlett.43.267
7. Vieira J, Martins SF, Fiuza F, Huang CK, Mori WB, Mangles SPD, et al. Influence of realistic parameters on state-of-the-art laser wakefield accelerator experiments. *Plasma Phys Control Fusion* (2012) 54:055010. doi:10.1088/0741-3335/54/5/055010
8. Albert F, Couprie ME, Debus A, Downer MC, Faure J, Flacco A, et al. 2020 roadmap on plasma accelerators. *New J Phys* (2021) 23:031101. doi:10.1088/1367-2630/abcc62
9. Mendonça JT, Ali S, Thidé B. Plasmons with orbital angular momentum. *Phys Plasmas* (2009) 16:112103. doi:10.1063/1.3261802
10. Allen L, Beijersbergen MW, Spreeuw RJC, Woerdman JP. Orbital angular momentum of light and the transformation of Laguerre-Gaussian laser modes. *Phys Rev A (Coll Park)* (1992) 45:8185–9. doi:10.1103/physreva.45.8185
11. Andrews DL, Babiker M. *The angular momentum of light*. Cambridge: Cambridge University Press (2013).
12. Mendonça JT, Vieira J. Donut wakefields generated by intense laser pulses with orbital angular momentum. *Phys Plasmas* (2014) 21:033107. doi:10.1063/1.4868967
13. Vieira J, Mendonça JT. Nonlinear laser driven donut wakefields for positron and electron acceleration. *Phys Rev Lett* (2014) 112:215001. doi:10.1103/physrevlett.112.215001
14. Vieira J, Mendonça JT, Quéré F. Optical control of the topology of laser-plasma accelerators. *Phys Rev Lett* (2018) 121:054801. doi:10.1103/physrevlett.121.054801
15. Fonseca RA. *Lecture notes in computer science*, 2331. Berlin, Heidelberg: Springer (2002).
16. Panofsky WKH, Wenzel WA. Some considerations concerning the transverse deflection of charged particles in radio-frequency fields. *Rev Sci Instrum* (1956) 27:967. doi:10.1063/1.1715427